Available online at www.sciencedirect.com
ScienceDirect
Ceramics International 34 (2008) 15–21
CERAMICS INTERNATIONAL
www.elsevier.com/locate/ceramint

Sintering behaviour of cobalt ferrite ceramic

A. Rafferty *, T. Prescott, D. Brabazon

Department of Mechanical and Manufacturing Engineering, Dublin City University, Glasnevin, Dublin 9, Ireland

Received 20 February 2006; received in revised form 22 June 2006; accepted 14 July 2006
Available online 25 September 2006

Abstract

Pure cobalt ferrite ceramic powder was prepared using standard solid-state ceramic processing. Uniaxially pressed pure cobalt ferrite discs, sintered under isothermal ramp rate and single dwell time conditions, yielded a maximum theoretical density (%D_{th}) of <90%. Discs made from finer particle size powder yielded a %D_{th} of 91.5%. Based on dilatometry analysis, a sintering profile comprising non-isothermal sintering, and two-step sintering was devised, yielding discs with %D_{th} of 96%. Cylindrical rods of pure cobalt ferrite were cold iso-statically pressed and sintered according to the revised sintering profile. Pycnometry analysis was used to quantify the percentages of open and closed pores in the rods after sintering.

Keywords: A. Sintering; D. Ferrites

1. Introduction

Magnetic ceramics may be divided into one of three different classes; spinel ferrites, hexagonal ferrites and the rare earth ferrites (garnet materials) [1]. The soft ferrites crystallise in the spinel structure, the structure of which was derived from the mineral spinel ($MgOAl_2O_3$ or $MgAl_2O_4$) [2]. The magnetic spinel has the general formula $MO{\cdot}Fe_2O_3$ or MFe_2O_4 where M is the divalent metal ion, usually Ni, Co, Mn or Zn [1]. Ferromagnetism of metal elements such as Ni, Co, Mn or Zn is derived from the unpaired electron spins in their atoms. The highest magnetic moments and therefore the highest saturation magnetisations are to be found in the metals themselves. Ferrimagnetic ferrites, based on metal oxides suffer from a dilution effect of the large oxygen ions in the crystal lattice [3]. The oxygen ions also serve to insulate the metal ions and therefore greatly increase the resistivity, making the ferrite especially useful at higher frequencies.

More traditional solid-state sintering studies of cobalt ferrite are extremely rare in the literature. Studies of other ferrite systems, such as NiZn, and MgZn, are more common, where the principal variables are peak sintering temperature and sintering dwell time. Barba et al. [4], investigated the single step sintering of Cu–Ni–Zn ferrite and achieved densities of 94%. They noted that when densification reached ~90%, average grain size increased rapidly and densification slowed. Wang et al. [5], also investigated nano-crystalline Ni–Cu–Zn ferrite, using the two-step sintering approach put forward by Chen and Wang [6]. Using this approach, densities >96% were achieved, and grain growth was suppressed in the final stage of densification. Kim and Han [7] adopted a similar approach to sinter nano-crystalline $BaTiO_3$. Some years previously, Ragulya [8] employed rate-controlled synthesis and rate-controlled sintering (RCS) to achieve 99.9% relative density and a grain size of 0.1–0.3 μm from nano-crystalline barium titanate powder. RCS was developed by Palmour and Huckabee [9], and is a form of non-isothermal, non-linear sintering where there is a feedback between densification and heating rate. In RCS, the green ceramic is sintered using a sintering cycle comprising at least three rate regimes. The densification rate in each regime is controlled so that it remains below the critical rate at which gas entrapment is effected and at which discontinuous grain growth is induced [9]. By varying the sample temperature it is attempted to adjust the real densification of the sample to a given densification profile. If real density drops below the set density the temperature is raised, to achieve a higher densification rate and vice versa. Very recently, Polotai et al. [10] employed a novel approach, combining two-step sintering and RCS, to sinter nano-crystalline $BaTiO_3$. By fully optimising their sintering steps,

* Corresponding author. Tel.: +353 1 7007776; fax: +353 1 7005345.
E-mail address: aran.rafferty@dcu.ie (A. Rafferty).

0272-8842/$32.00
doi:10.1016/j.ceramint.2006.07.012

a fully dense ceramic (relative density 99.7%) with an average grain size of 108 nm was produced. Polotai et al. found grain growth coefficients of 66 and 12, respectively, for conventional sintering and non-isothermal RCS. When these two approaches were combined this coefficent reduced further to 3.5. Positive findings for the RCS approach have also been found by other authors [8,11,12]. However, Zagirnyak et al. [13] used RCS for sintering of strontium ferrite and reported only modest values of 92–95% theoretical density.

In terms of applications, the spinel-type ferrites are commonly utilised in fine electronic devices owing to their remarkable magnetic and semiconducting properties [14]. Cobalt ferrite was rarely considered as a permanent magnet material mainly because of its low coercivity [15]. However, nano-crystalline cobalt ferrite has recently been reported as a hard magnetic material due to its high coercivity (5400 Oe) as compared with co-ferrite prepared via conventional powder sintering [16]. There has been a surge in research activity into ultrafine cobalt ferrite preparation techniques, in particular the sol–gel method [17–19], but also by an emulsion method [20] and by complexometric synthesis [21]. One major driving force for this activity is the potential use of cobalt ferrite as high-density storage media where the ferrite particles must be less than 10 nm to avoid exchange interactions between neighbouring grains [22]. Wang et al. [5] point out, however, that in general, present day ferrite manufacturing technologies typically result in micrometer size grains. For Ni–Cu–Zn ferrites a key area of advantage of smaller particles is the manufacture of multi-layer-chip capacitors or multi-layer-chip inductors, where layers are becoming increasingly thinner. As the grain size should be no more than one-tenth of the layer thickness, nanograin ceramics will be required. Furthermore, the lower sintering temperature associated with two-step sintering will better satisfy the requirements for co-firing with lower cost Ag electrodes [5].

Chen et al. [23] have studied cobalt ferrite and metal-bonded cobalt ferrite composites, for potential use as a new magnetomechanical sensor material. Cobalt ferrite is a magnetostrictive material and undergoes a dimensional change when exposed to a magnetic field [24]. According to Chen, these materials show a steep slope of magnetostriction at low applied fields, $(d\lambda/dH)_{\sigma}$, which contributes to a high sensitivity of magnetic induction to stress, hence giving high signal-to-background noise ratios in sensor applications. The measured magnetostriction of $CoFe_2O_4$ peaks at relatively low field (300 kA/m), then decreases with increasing field, as the magnetisation of the particles or grains is rotated away from the $\langle 1\,0\,0 \rangle$ easy axis direction. Chen et al. found that metal-bonded cobalt ferrite composites offered better mechanical properties and a higher slope at low applied field (<100 kA/m) and were thus considered better candidates for sensor and actuator applications, despite exhibiting lower peak magnetostriction than pure cobalt ferrite. In terms of sintering, Chen et al. [23] cold pressed the micron-sized cobalt ferrite powder into shapes and sintered up to 1450 °C. Elsewhere [25] they described sintering in air at 4 °C/min to 1400 °C, then furnace cooling.

2. Experimental procedure

2.1. Cobalt ferrite preparation

Cobalt ferrite powder was prepared by blending stoichiometric amounts of high purity cobalt oxide (CoO) and iron oxide (Fe_2O_3) powders in a conventional ball mill. A 788 cc mill was used with 718 g of 20 mm diameter alumina balls. This was particularly effective in breaking up large pieces of iron oxide. The powder mixture was then sieved to <150 μm, placed in alumina crucibles (Almath Ltd., UK) and fired in a horizontal tube furnace at 1000 °C for 72 h in flowing dry air to form the compound ($CoFe_2O_4$). After firing, the powder compound was then re-sieved to <150 μm. Using a mixer and hotplate, 3 wt% PVA and 3 wt% glycerine was dissolved in distilled water. The cobalt ferrite powder was blended into this solution and mixed thoroughly. The mixture was placed on evaporating dishes, dried at 95 °C, ground using a mortar and pestle and re-sieved to <150 μm. For the sample containing silver and nickel, the powders were added as 2 vol% $Ag_{0.97}Ni_{0.03}$ during the binder addition step.

2.2. Disc formation and sintering

Discs were formed by uniaxially pressing 3.0 g of powder in a 26 mm diameter steel die. A load of 20 kg/cm^2 was applied for a duration of 20 s. A horizontal tube furnace (Carbolite, Sheffield, UK) was used to fire the discs which were loaded on alumina tiles. Binder burnout was carried out at 0.1 °C/min to 550 °C, held for 1 h at 550 °C and then cooled to room emperature at 3 °C/min. The sintering dwell time employed was 3 h. The heating and cooling rates were 10 °C/min.

The geometric green and sintered density of each cylindrical pellet was calculated on the basis of mass and volume measurements, using a precision balance (accuracy 0.0001 g) and vernier calipers (accuracy 0.01 mm), respectively. An average thickness was determined from four measurements. Diameter values were calculated as the average of two measurements. Percentage theoretical density ($\%D_{th}$) calculations were made using the formula:

$$\%D_{th}\,(g/cm^3) = \text{measured density}/\text{theoretical density}$$

The theoretical density of $CoFe_2O_4$ was calculated taking the molecular weight of $CoFe_2O_4$ to be 234.63 g. Spinel ferrites have eight formula units per unit cell. Therefore, the molecular weight of one cell is $8 \times (234.63) = 1877.04$ g. The volume of a cube of side, length a is a^3. The volume of a cell is therefore $A \times a^3$ where A is Avogadro's number. The unit cell edge a_0 (Å) of $CoFe_2O_4 = 8.38$ therefore $a^3 = 588.48$ Å^3. As 1 Å$^3 = 10^{-24}$ cm^3, $A \times a^3$ is therefore:

$$[6.023 \times 10^{23}][588.48 \times 10^{-24}] = 354.44\,cm^3$$

Density = mass/volume = 1877.04/354.44 = 5.2957 g/cm^3

2.3. Attrition milling

Cobalt ferrite powder was attrition milled using a Netzsch attrition mill (Netzsch Ltd., Germany) which incorporated an alumina grinding tank and grinding shaft. 1 mm diameter zirconia media was added to the powder dispersed in propan-2-ol. A grinding shaft speed of 1500 rpm for 1 h was used throughout. Two experiments were conducted; one employed a media to powder ratio of 2:1 (400 g media, 200 g powder) the other a media to powder ratio of 10:1 (400 g media, 40 g powder). After milling, the suspensions were dried at 95 °C and the powder sieved through a 150 μm mesh.

2.4. Particle size analysis

Particle size analysis of powders was carried out using a Mastersizer S particle size analyser (Malvern Instruments, UK). Powders were dispersed in water, to which a few drops of calgon solution was added as a dispersant. A standard wet dispersion unit equipped with ultrasonics was used to circulate the powder suspension through the sample cell.

2.5. Dilatometry analysis

Dilatometry was conducted using a Netzsch dilatometer (Netzsch Ltd., Germany). Rectangular bars (20 mm × 5 mm × 2 mm) were uniaxially pressed and used as samples. A heating rate of 10 °C/min was employed to 1470 °C.

2.6. Cold iso-static pressing

Rods were cold iso-statically pressed using a wet-bag isostatic press (Stansted Fluid Power Ltd., UK). Rubber bags were procured from Trexler Rubber Ltd. (Ohio, USA). During filling, the rubber bag was encased in a cardboard tube to prevent bulging of the bag. The bag was tapped during filling to aid compaction. A plunger was also used to compact the powder in the bag. A vacuum pump and bung were used to remove the air from the bag, thus providing an initial pre-pressing. The pressure profile used to isostatically press the rods is shown in Fig. 1.

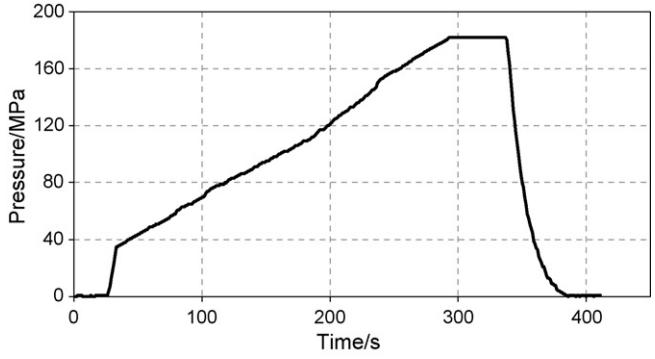

Fig. 1. Cold iso-static pressing pressure profile.

2.7. Helium pycnometry

Density measurements were performed on sintered discs using an AccuPyc 1330 helium gas pycnometer (Micromeritics, USA). The analysis measures sample volume, from which density is derived after sample weight has been entered.

2.8. XRD analysis

XRD was conducted on the fired $CoFe_2O_4$ powder using Cu Kα X-rays (Philips, UK).

3. Results and discussion

The preparation of cobalt ferrite by firing mixed cobalt oxide and iron oxide powders in air at 1100 °C has previously been described by Chen et al. [23]. No other firing temperatures were described by those authors. In this work, tests were performed to assess the feasibility of firing the compound at a lower temperature. It was felt that some sintering could occur at 1100 °C, leading to lumps which might be difficult to break down. For this reason, a firing temperature of 1000 °C was considered more appropriate. XRD traces of cobalt ferrite fired at 1000 and 1100 °C were identical, thus confirming the 100% conversion to cobalt ferrite on firing at 1000 °C. Fig. 2 shows the resultant XRD pattern after firing at 1000 °C.

Pycnometry was performed on a powder sample of the cobalt ferrite and a density of 5.24 g/cm^3 was recorded. This value was in good agreement with the theoretical density of $CoFe_2O_4$ of 5.2957 g/cm^3, calculated previously.

An average green theoretical density of 56% (%D_{th}) for pressed discs was recorded. Sintering trials were conducted on these discs in the temperature range 1200–1500 °C. Fig. 3 graphs the theoretical density of these discs as a function of sintering temperature.

As can be seen from Fig. 3, the %D_{th} increases as the sintering temperature is increased. At higher temperatures, a plateau region is reached, where no significant increase in sintering takes place. A %D_{th} of 88.67% was reached at 1450 °C. Hold times greater than 3 h did not improve the theoretical density. A 3 h hold at 1500 °C caused a slight decrease in %D_{th}.

Particle size analysis revealed that after ball-milling and sieving, the base powder mix had an average particle size of

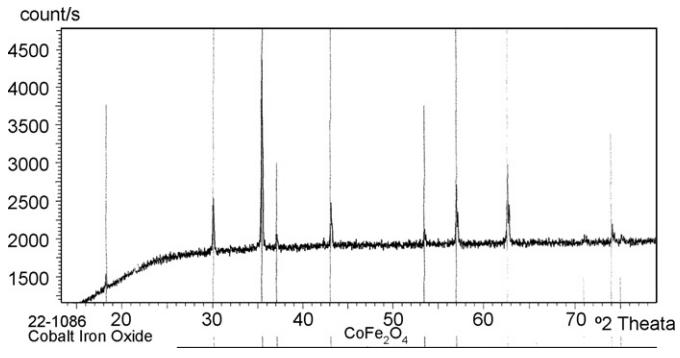

Fig. 2. XRD analysis of $CoFe_2O_4$, following heat treatment for 72 h at 1000 °C. JCPDS pattern 22–1086, 11 lines observed.

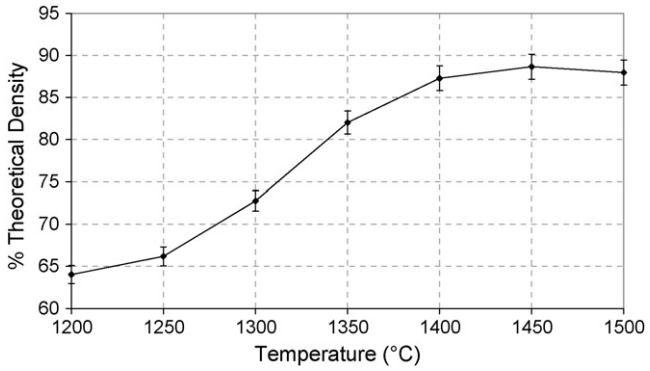

Fig. 3. Theoretical density versus sintering temperature for cobalt ferrite discs for a 3 h dwell time (S.D. ± 1.67%).

14.17 μm. Attrition milling was carried out in an attempt to produce finer particles, thus leading to higher packing density. For uniformly compacted fine powders the rate of densification is higher than for a similar system with heterogeneous packing. The finer particle size results in a higher surface energy for a compact, and thus a higher driving force for grain growth (growth of crystallites) and densification to reduce the system's Gibbs energy [26]. Attrition milling is an efficient way to reduce coarse particles to micron sizes (1–10 μm), but an inefficient way to obtain submicron particles (<1 μm). One disadvantage of attrition milling is the possibility of contamination from grinding media and grinding tank. Fig. 4 shows particle size distributions for attrition milled and non-attrition milled cobalt ferrite powder. Table 1 shows the average particle sizes D [4,3] obtained:

Increasing the quantity of media led to more narrow powder particle distributions. However, with this approach, only small quantities of powder could be used. Coupled with the inevitable powder losses incurred during milling, this approach was not considered feasible. To mill large batches of cobalt ferrite, a 2:1 ratio of media to powder was considered a feasible option. The resultant 5.34 μm particle size powder had a surface area of 0.7381 m^2/g as measured using BET surface area analysis.

The densification behaviour of bar-shaped samples made from the attrition milled powders was investigated using dilatometry, see Fig. 5.

For the base powder (14.71 μm), shrinkage onset commences in the region of 900 °C whilst the overall linear shrinkage is approximately 12%. However, the shrinkage has not fully

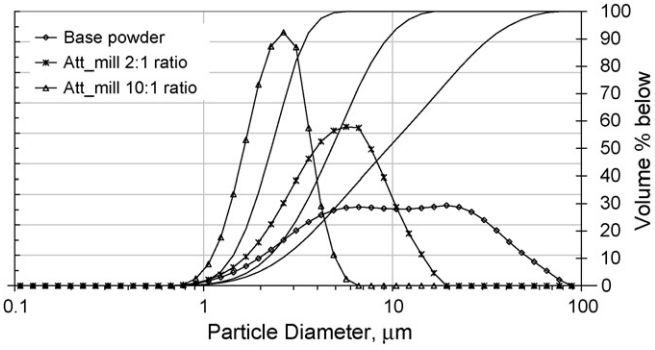

Fig. 4. Particle diameter of non-attrition milled and attrition milled powders using different media-powder milling ratios.

Table 1
Average powder particle sizes before and after attrition milling

	Base powder	Attrition 2:1	Attrition 10:1
D[4,3] (μm)	14.17	5.34	2.37

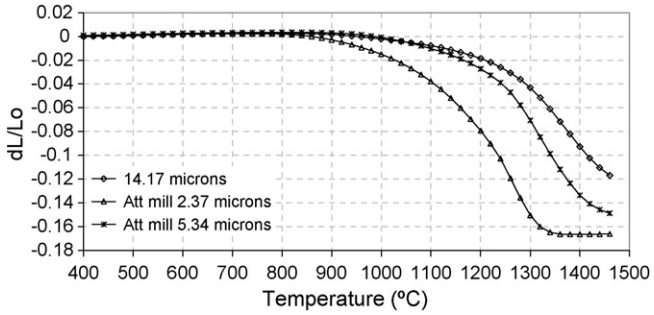

Fig. 5. Shrinkage of cobalt ferrite as a function of particle size.

completed for an isothermal run to 1470 °C; the curve has not flattened out. For the 5.34 μm powder, the rate of shrinkage is sharper with a final linear shrinkage of approximately 15%. For the 2.37 μm powder sample, shrinkage commences at lower temperatures with full shrinkage completed by 1350 °C.

Discs were made from the different particle size powders and the $\%D_{th}$ measured using a geometrical approach, see Table 2. Pycnometry analysis was also employed. Based on these methods, assumptions could be made regarding the type of porosity present. The geometrical approach provides a value for bulk density and is thus unable to differentiate between open or closed porosity. However, in pycnometry, helium gas will penetrate all but closed pores thus yielding a value of skeletal density. From the difference between bulk and skeletal densities, the percentages of closed and open pores can be approximated.

From Table 2, it can be seen that the $\%D_{th}$ increases by >4% as the particle size is decreased from 14.17 to 5.34 μm. No further increase in the $\%D_{th}$ is detectable when the particle size was further reduced. This was initially surprising, in light of the dilatometry data, which shows an increase in linear shrinkage for this particle size. However, pycnometry of this sample yielded 96.68 $\%D_{th}$. This result revealed that the sample consisted of 5.27% open porosity and 3.32% closed porosity. In comparison the 14.17 μm sample consisted of 2.94% open porosity and 9.95% closed porosity. This indicated that for this larger particle size a process of de-sintering was occurring resulting in rapid grain growth and pore entrapment.

Table 2
Percentage theoretical densities of discs sintered for 3 h at 1450 °C

Grade	Pure (14.17 μm)	Attrition mill (5.34 μm)	Attrition mill (2.37 μm)
$\%D_{th}$ calipers	87.51	91.62	91.41
$\%D_{th}$ pycnometer	90.45	92.76	96.68
Open porosity (%)	2.94	1.14	5.27
Closed porosity (%)	9.55	7.24	3.32

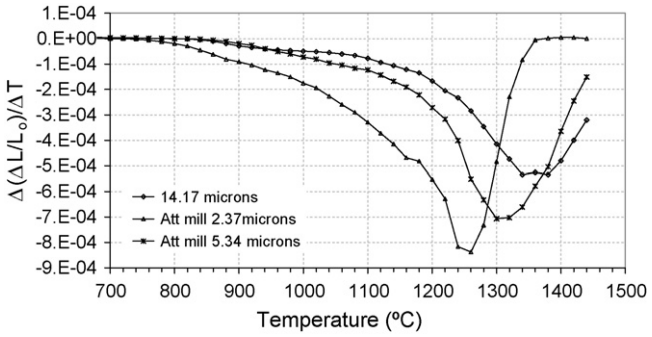

Fig. 6. Differential shrinkage curves.

From these findings it was concluded that decreasing the particle size, coupled with an isothermal sintering profile, was not in itself enough to affect an increase in $\%D_{th}$. Open interconnected porosity was not being completely eliminated. The percentage of closed pores was high. Ideally only very isolated closed pores would exist. However, it was noted that the $\%D_{th}$ of 96.68% was a satisfactory one and elimination of open porosity via an optimised sintering profile should deliver this bulk density value.

In an attempt to better understand the densification processes taking place, differential shrinkage curves were plotted from dilatometry data, see Fig. 6.

From Fig. 6, the temperature ranges of maximum shrinkage can be observed. For example, for the 2.37 μm powder, a densification rate peak occurs at 1260 °C. For the 5.34 μm powder this shifts to approximately 1310 °C. On this basis, it was felt that the sintering temperature of 1450 °C was not optimal, in terms of achieving maximum density. By heating at 10 °C/min to 1450 °C the critical densification stage was in effect being bypassed.

This intermediate stage of sintering commonly refers to the stage between approximately 65% and 90 $\%D_{th}$ [27]. In this stage, pores are connected and discrete necks exist between the particles. Densification only takes place if mass is transported from the particle volume or grain boundary to the neck forming region between particles. If the only material transport mechanism originates on the surface of particles, no shrinkage will take place. In this case, a change of shape and size of particles and pores occurs, causing grain growth. This occurrence depletes the system of surface energy and effectively prevents the densification of the compact. One solution to this is the use of two-step sintering, where the first stage produces a uniform pore microstructure, prior to second stage sintering. Wang et al. [5] carried out an extensive two-step sintering study of Ni–Cu–Zn ferrite and determined that a critical lowest starting density of 76% was required after the first sintering step to enable high densities (>96.2%) to be achieved after the second step. Below the critical density the pore size is so large, compared with the grain size, that pores are thermodynamically stable and won't close. Above the critical density, all pores become subcritical and unstable against shrinkage. Wang et al. [5] found similar second step sintering mechanisms for the Y_2O_3, $BaTiO_3$ and Ni–Cu–Zn systems.

For the 2.37 μm powder sample in Fig. 6, the sintering has completely finished at 1450 °C, so holding at this temperature for 3 h is likely to have a negative effect, leading to exaggerated grain growth and pore entrapment. In the final stage of sintering ($>\approx$90% D_{th}) porosity should be eliminated. This can only happen if all pores are connected to fast, short diffusion paths along grain boundaries. For this to happen, any pores must follow the movement of grain boundaries. If discontinuous grain growth occurs then pores become trapped inside large grains. These pores are difficult to remove due to diffusion paths being long and slow, as lattice diffusion is the controlling mechanism. Open porosity effectively impedes grain boundary migration. In the final stage of sintering, the open porosity network loses stability, forming closed spherical or ellipsoidal pores, which are located in triple junctions. Splitting of cylinder-shaped pores and localisation of spherical pores are accompanied by extended grain growth [10]. Some authors have gone to great lengths [5,10] to accurately determine the relative density boundary value at which to switch to the second stage of two-step sintering. For example, Polotai et al. [10] found 94% to be optimum for the barium titanate system they studied.

Another possible reason for trapped pores in the samples studied here is inadequate removal of gaseous products generated by the decomposition of organic binder substances. According to Lewis [28], carbon retention, cracking, blistering, warping, anisotropic shrinkage, and delamination of fired bodies can all result from inadequate binder removal. Successful debinding of ceramic green bodies requires a delicate balance between the generation rate of volatile constituents and their removal rates and the minimization of sharp concentration (hence, stress) gradients within the porous body to avoid the formation of defects.

Based on the differential shrinkage curve in Fig. 6, a two-step sintering profile was devised for the 5.34 μm powder. Fig. 7 shows one sintering profile that was used, consisting of a 3 h hold at 1310 °C, a ramp rate of 20 °C/min to 1450 °C and a 30 min hold at 1450 °C. This was followed by cooling at 5 °C to room temperature.

Based on this (and similar) two-step sintering profiles, discs were sintered. Table 3 shows the results obtained. As can be seen, a dramatic increase in $\%D_{th}$ was observed, with values of 95–96% recorded. Pycnometry data yielded a maximum $\%D_{th}$ of 97.94%, indicating that yet higher densities could be achieved, on successful removal of all open porosity.

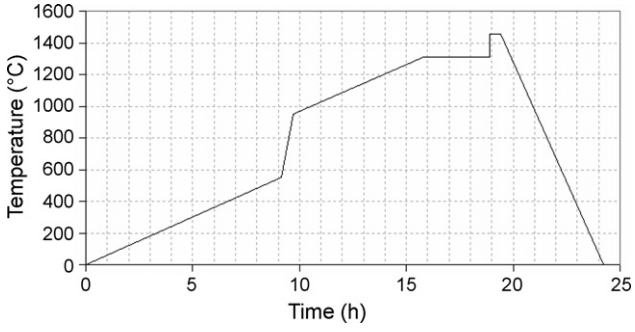

Fig. 7. Optimised sintering profile.

Table 3
Theoretical densities recorded for discs sintered using the modified, non-isothermal, two-step sintering profiles

Disc sinter conditions	1 h 1310 °C, 30 min at 1500 °C	3 h 1310 °C, 30 min at 1500 °C	3 h 1310 °C, 3 h at 1500 °C	6 h 1310 °C, 3 h at 1500 °C
$\%D_{th}$ callipers	95.22	95.55	95.92	96.21
$\%D_{th}$ pycnometer	96.59	97.16	97.94	96.30
Open porosity (%)	1.37	1.61	2.02	0.09
Closed porosity (%)	3.41	2.84	2.06	3.7

In their single step sintering study of Cu–Ni–Zn ferrite, Barba et al. [4] advocate a rate-controlled methodology based on equations relating densification to grain growth. They use the expression:

$$r = 15.0 \exp\left(\frac{2449}{T}\right) \frac{(1-\Phi_c)^{4/3}}{\eta} \quad (1)$$

to predict whether densification will occur, where r is the rate ratio, defined as the quotient of densification rate ($d\phi_c/dt$) to grain growth rate ($d\eta/dt$), ϕ_c is the relative density, T the sintering temperature and η is a dimensional average grain size. For $r > 1$, the densification rate will exceed the grain growth rate whereas for $r < 1$ the grain growth rate will exceed the densification rate leading to abnormal grain growth. From Eq. (1), r will decrease as the sintering temperature rises. For a given relative density, r will decrease with an increase in grain size. Finally, at a given average grain size, r decreases with increasing relative density so that for >90% D_{th}, densification is inhibited. Based on the above, Barba et al. [4] claim that when relative density has reached critical values ($\phi_c \approx 90\%$), temperature should be decreased and dwell time increased, to maximise the potential for complete densification.

The optimised sintering profile adopted for the cobalt ferrite in this work is not unlike the two-step sintering approach recommended by Barba et al. [4], and carried out by Kim [7] and others [5,29]. The major advantage of two-step sintering, as conceived by Chen and Wang [6], is the ability to achieve dense, nanostructured materials of grain size 25–30 nm from powders of size range 5–10 nm. In Polotai et al.'s [10] study of nano-crystalline barium titanate, the goal of the first stage of two-step sintering was to produce and freeze in place a uniform pore microstructure while minimising grain growth. This fine and uniform microstructure minimises diffusion distance during constant grain-size sintering which maximises densification kinetics leading to almost fully dense ceramics (99.7 $\%D_{th}$). It is known that the transverse rupture strength of a sintered ceramic body is proportional to $1/\sqrt{d}$, where d is the grain diameter. The ability to form almost fully dense bodies, with small grain sizes by two-step sintering presents a major advantage over hot pressing, in terms of cost and particularly for large commercial scale production of ceramic articles.

In this work, the isothermal hold part of the two-step sintering is implemented as part of the heating cycle, not the cooling. In order to further test this sintering profile, rods were cold isostatically pressed and sintered. After sintering, the rods were machined using a lathe in an attempt to produce uniform cylinders. A rod containing Ag/Ni was the only rod which survived the machining process. Fortunately, it was possible to grind pieces of the fractured rods into cylinders to facilitate density measurements. This data is shown in Table 4. A $\%D_{th}$ value of 91.49% was recorded for the Ag/Ni containing rod made in this work. This is high compared with 83.91% recorded for the rod made from the same particle size powder but containing no Ag/Ni. Chen et al. [23] use additions of Ag/Ni to wet the ferrite, thus improving the properties of the Co-ferrite by producing a stronger bond. Presumably, the Ag/Ni as a liquid phase, fills many of the pores created by the deleterious isothermal, single step sintering. However, it is unlikely that this is the only reason for the poor mechanical strength of the rods.

The $\%D_{th}$ density of the rods made using the optimised sintering profile was approximately 92%. This value is considerably lower than the ~96% values recorded for the equivalent discs. One explanation could be less efficient removal of the PVA binder from the larger sample, leading to trapped pores. This theory is strengthened by the fact that the thicker 30 × 50 mm rod showed such a poor $\%D_{th}$ despite being made from fine 5.34 μm powder. It should be more difficult to remove binder from larger samples.

With the final rod, great care was put into isostatically pressing to produce a smooth cylinder. Rather than using a lathe, the ends of the rod were then ground flat to produce a perfect cylinder. The $\%D_{th}$ as measured geometrically was 92.54%. The rod was too large to fit in the sample chamber to allow for pycnometry analysis.

Table 4
Pycnometry measurements of cylindrical section of iso-statically pressed Co-ferrite rods

Rod dimension (mm) and powder particle size (μm)	20 × 100 (14.17) (Ag/Ni)	20 × 100 (14.17)	30 × 50 (5.34)	20 × 100 (5.34) OSP	20 × 100 (5.34) OSP
Calipers $\%D_{th}$	91.49	83.91	85.27	91.16	92.54
Pycnometry $\%D_{th}$	92.66	85.69	90.41	91.87	–
Closed pores (%)	7.34	14.31	9.59	8.13	–
Open pores (%)	1.17	1.78	5.14	0.71	–

OSP: optimised sintering profile.

Encouraging $\%D_{th}$ values were obtained for the rods sintered using the optimised profile. Also, for one of the rods at least, only 0.71% open porosity was present. This indicates that the interconnected, open porosity is being closed by holding at lower dwell temperatures. Of concern is the high percentage, 8.13, of closed pores. This can be attributed to trapped binder, exaggerated grain growth, or a combination of the two.

Duran et al. [30] using porosimetry analysis to investigate micron-sized barium titanate, found that for intermediate stage sintering (>1000 °C), both the total pore volume and the average pore size decreased, in accordance with the concept of equilibrium pore size proposed by Kingery and Francois [31]. According to Duran et al., the end of the intermediate stage of sintering occurred at 92 $\%D_{th}$, and this is characterised by a transition from continuous pore channels to isolated pores. Polotai et al. [10], in their study of nanosized $BaTiO_3$, use the $\%D_{th}$ value of 94% as the point for switching to the two-step sintering regime. They claim that this density is the transition point between the open and closed porosity networks and the onset point for extended grain growth. In fact, this very recent approach employed by Polatai et al. [10] comprising RCS as part of a two-step, atmosphere controlled sintering profile is of major significance. In their study, powder of <40 nm particle size is pressureless sintered to full density with final grain sizes of ~100 nm. Future work on cobalt ferrite sintering could try to establish an optimum sintering profile similar to the approach employed by Polotai et al. [10], and in this way it is likely that the degree of closed porosity could be further reduced.

4. Conclusions

A two-step sintering profile is described which can produce cobalt ferrite discs with a $\%D_{th}$ of ~96%. Analysis of differential shrinkage curves was found to be key in determining the optimum sintering profile. Pycnometry analysis was found to be a useful technique in terms of investigating percentages of open and closed porosity. Using the revised sintering profile, cylindrical rods of length 100 mm and diameter 20 mm were cold isostatically pressed and sintered to a $\%D_{th}$ of approximately 92%.

Acknowledgements

This work was supported by the European Commission through the IELAS project (contract number G5RD-CT-2001-0054) under the Competitive and Sustainable Growth Research Programme. This support is gratefully acknowledged.

References

[1] R.E. Loehman, Characterization of Ceramics, Butterworth-Heinemann, Massachusetts, 1993.
[2] A. Goldman, Modern Ferrite Technology, Van Nostrand Reinhold, New York, 1990.
[3] R. Valenzuela, Magnetic Ceramics, Cambridge University Press, Great Britain, 1994.
[4] A. Barba, C. Clausell, C. Feliu, M. Monzo, Sintering of $(Cu_{0.25}Ni_{0.25}Zn_{0.50})Fe_2O_4$ ferrite, J. Am. Ceram. Soc. 87 (2004) 571–577.
[5] X.H. Wang, X.Y. Deng, H.L. Bai, H. Zhou, W. Qu, L.T. Li, Two-step sintering of ceramics with constant grain-size, II: $BaTiO_3$ and Ni–Cu–Zn ferrite, J. Am. Ceram. Soc. 89 (2005) 438–443.
[6] I.W. Chen, X.H. Wang, Sintering dense nanocrystalline ceramics without final-stage grain growth, Nature 404 (2000) 168–171.
[7] H.T. Kim, Y.H. Han, Sintering of nanocrystalline $BaTiO_3$, Cers. Int. 30 (2004) 1719–1723.
[8] A.V. Ragulya, Rate-controlled synthesis and sintering of nanocrystalline barium titanate powder, Nanostructured Mater. 10 (1998) 255–349.
[9] H. Palmour III, M.L. Huckabee, Process for sintering finely divided particulates and resulting ceramic products, US patent No. 3900542, August 19th, 1975.
[10] A. Polotai, K. Breece, E. Dickey, C. Randall, A novel approach to sintering nanocrystalline barium titanate ceramics, J. Am. Ceram. Soc. 88 (2005) 3008–3012.
[11] A.V. Ragulya, V.V. Skorokhod, Rate-controlled sintering of ultrafine nickel powder, 5 (1995) 835–843.
[12] O.B. Zgalat-Lozinskii, V.N. Bulanov, I.I. Timofeeva, A.V. Ragulya, V.V. Skorokhod, Sintering of refractory compounds nanocrystalline powders. II. Non-isothermal sintering of titanium nitride powder, Powder Metall. Met. Cers. 40 (2001) 573–581.
[13] M.V. Zagirnyak, L.N. Tuilchinsky, V.M. Letschinsky, IEEE (1998) 340–343.
[14] M. Soliman Selim, G. Turky, M.A. Shouman, G.A. El-Shobaky, Effect of Li_2O doping on electrical properties of $CoFe_2O_4$, Solid State Ionics 120 (1999) 173–181.
[15] S.R. Mekala, J. Ding, Magnetic properties of cobalt ferrite/SiO_2 nanocomposite, J. Alloy Compd. 296 (2000) 152–156.
[16] P.C. Dorsey, P. Lubitz, D.B. Chrisey, J.S. Horwitz, $CoFe_2O_4$ thin films grown on (1 0 0) MgO substrates using pulsed laser deposition, J. Appl. Phys. 79 (1996) 6338.
[17] J.G. Lee, J.Y. Park, C.S. Kim, Growth of ultra-fine cobalt ferrite particles by a sol–gel method and their magnetic properties, J. Math. Sci. 33 (1998) 3965–3968.
[18] J.G.S. Duque, M.A. Macedo, N.O. Moreno, J.L. Lopez, H.D. Pfanes, Magnetic and structural properties of $CoFe_2O_4$ thin films synthsized via a sol–gel process, J. Magn. Magn. Mater. 226–230 (2001) 1424–1425.
[19] J.G. Lee, J.Y. Park, Y.J. Oh, C.S. Kim, Magnetic properties of $CoFe_2O_4$ thin films prepared by a sol–gel method, J. Appl. Phys. 84 (1998) 2801–2804.
[20] L. Zhao, H. Yang, X. Zhao, L. Yu, Y. Cui, S. Feng, Magnetic properties of $CoFe_2O_4$ ferrite doped with rare earth ion, Mater. Lett. 60 (2006) 1–6.
[21] P.D. Thang, G. Rijnders, D.H.A. Blank, Spinel cobalt ferrite by complexometric synthesis, J. Magn. Magn. Mater. 295 (2005) 251–256.
[22] E.S. Murdock, R.F. Simmons, R. Davidson, Roadmap for 10 Gbit/in.^{2} media: challenges, IEEE Trans. Magn. 28 (1992) 3078.
[23] Y. Chen, J.E. Snyder, C.R. Schwichtenberg, K.W. Dennis, R.W. McCallum, D.C. Jiles, Metal-bonded co-ferrite composites for magnetostrictive torque sensor applications, IEEE Trans. Magn. 35 (1999) 3652–3654.
[24] E. du Trémolet, de Lacheisserie, Magnetostriction: Theory and Applications of Magnetoelasticity, CRC Press, Boca Raton, 1993.
[25] R.W. McCallum, J.E. Snyder, K.W. Dennis, C.R. Schwichtenberg, D.C. Jiles, Ames Laboratory, US Patent 6,352,649, March 5th, 2002.
[26] D. Kolar, Chemical research needed to improve high-temperature processing of advanced ceramic materials, Pure Appl. Chem. 72 (8) (2000) 1425–1448.
[27] M.N. Rahaman, Ceramic Processing and Sintering, Marcel Dekker Inc.,, New York, 1995.
[28] J.A. Lewis, Binder removal from ceramics, Annu. Rev. Mater. Sci. 27 (1997) 147–173.
[29] X.-H. Wang, P.-L. Chen, I.-W. Chen, Two-step sintering of ceramics with constant grain size. 1. Y_2O_3, J. Am. Ceram. Soc. 89 (2006) 431–437.
[30] P. Duran, J. Tartaj, C. Moure, Sintering behaviour and microstructural evolution of agglomerated spherical particles of high-purity barium titanate, Cers. Int. 29 (2003) 419–425.
[31] W.D. Kingery, B. Francois, Grain growth in porous compacts, J. Am. Ceram. Soc. 48 (1965) 546–547.